Geomechanics and Engineering, *Vol. 43, No. 1 (2025) 13-26*
https://doi.org/10.12989/gae.2025.43.1.013

Mechanical and hydraulic improvement of highly organic soil using Xanthan Gum: A strength–microstructure approach

Muhammad Hamza*[1,2] and Muhammad Israr Khan[1,2,3]

[1]*College of Civil and Transportation Engineering, Shenzhen University, Shenzhen 518060, China*
[2]*State Key Laboratory of Intelligent Geotechnics and Tunnelling, Shenzhen University, Shenzhen 518060, China*
[3]*Key Laboratory for Resilient Infrastructures of Coastal Cities, Shenzhen University, Shenzhen 518060, China*

(*Received June 30, 2025, Revised September 3, 2025, Accepted September 26, 2025*)

Abstract. Highly organic soils are often challenging for geotechnical applications due to their low strength, high compressibility, and increased permeability. This study investigates the efficacy of xanthan gum (XG) biopolymer as an eco-friendly alternative to traditional, carbon-intensive soil stabilizers. A comprehensive series of laboratory experiments was conducted to assess the effects of XG on the compaction behavior, unconfined compressive strength (UCS), elastic modulus (E_{50}), and permeability of organic soils. XG dosages ranged from 0% to 5% (by dry weight of soil), with aging periods extending up to 60 days. The test results demonstrate that 1% XG significantly improves the mechanical properties of the soil, achieving a sixfold increase in UCS and E_{50} greater than 20,000 kPa within 28 days of aging. Additionally, permeability was reduced by 3–5 orders of magnitude, meeting the stringent requirements for hydraulic barrier applications. Scanning electron microscopy (SEM) identified the formation of a bridging gel matrix and associated pore-clogging as the key microstructural mechanisms responsible for the significant gains in strength and the drastic reduction in permeability. Based on the analysis of strength, stiffness, and permeability, 1% XG was identified as the optimal dosage. These findings highlight the significant potential of XG as a sustainable, cost-effective solution for stabilizing highly organic soils, offering substantial performance enhancement while maintaining environmental benefits. XG presents a viable alternative to conventional stabilizers in geotechnical applications, particularly in projects requiring environmentally conscious and efficient material solutions.

Keywords: biopolymer; compaction behavior; elastic modulus; organic soils; permeability reduction; scanning electron microscopy; soil stabilization; sustainable geotechnical materials; unconfined compressive strength; Xanthan gum

1. Introduction

Mass excavation, dredging, and urban renewal projects generate large volumes of marginal soils with low strength, high compressibility, and high permeability, making direct reuse impractical and disposal costly (Blanck *et al*. 2014). Conventional binders (lime/cement/fly ash) improve reuse, but their carbon footprint and alkalinity motivate natural-polymer alternatives, particularly for highly organic soils where field performance data remain limited (Aziz *et al*. 2021). Conventional soil stabilizers can change the pH of stabilized soil, resulting in severe environmental implications such as slower vegetation growth, decreased groundwater resources, and even public medical issues (Chang *et al*. 2015). Cement production is one of the world's largest sources of harmful carbon dioxide (CO_2) gas emissions, with one ton of CO_2 produced for every ton of cement produced; as a result, it is estimated that cement production accounts for 5% of global CO_2 emissions annually (Chang *et al*. 2015). Particulate air emission in the form of cement dust is another ecological concern. Vast quantities of unwanted concrete dust are released due to earthquakes and buildings demolition (Meo 2004). To address these environmental concerns, some scientists have lately focused on using modern soil stabilizers, which can give a better long-term solution for particular applications (Ali *et al*. 2020, Biju and Arnepalli 2020, Hamza *et al*. 2022, Qureshi *et al*. 2021, Rasool *et al*. 2023).

Biogeotechnology is a new field of geotechnical engineering concerned with the practical implementation of bacterial methods to create additives that improve weak geomaterials (soft, organic, collapsible and expansive soils). Biogeotechnology provide lower initial and ongoing expenses, as well as more significant environmental benefits than their conventional soil stabilizing competitors (Ivanov and Chu 2008). Because geotechnical construction projects are frequently large-scale, mainly for land recovering projects, using a biologically based soil stabilizing agent can save funds in some cases, especially if the stabilizing agent is easily accessible in each region or is a by-product of another manufacturing process that must be coped with anyway.

Biopolymers are natural polysaccharides generated by fungus, bacteria, or algae that exhibit innate characteristics like high viscosity, resistance to shear degradation, stability, and pseudo-plasticity over a wide range of pH and temperature (Chudzikowski 1971, García-Ochoa *et al*. 2000, Moghal and Vydehi 2021). Furthermore, biopolymers do not contribute to harmful gas emissions because they

*Corresponding author, Ph.D.
E-mail: hamza30@qq.com

ISSN: 2005-307X (Print), 2092-6219 (Online)

Table 1 Biopolymer-stabilized soils: past findings and current contribution on highly organic soils

Source	Soil type	Biopolymer	Optimal dosage	Research results	Gap / Limitations
This Study	Highly organic soil	XG	1%	UCS increased sixfold (to 698 kPa at 60 days); $E_{50} \geq 20{,}000$ kPa (28 days); permeability reduced by 3 to 5 orders of magnitude; SEM confirmed pore clogging and gel bonding	First systematic evaluation of XG on highly organic soils; integrates strength–hydraulic–microstructural evolution with performance modeling and threshold-based decision mapping, offering a practical design framework
Sujatha *et al*. (2025)	Fine sand	XG, CMC	0.5% XG, 0.75% CMC	98–99% reduction in wind erosion; XG more durable under immersion	Study focused exclusively on erosion resistance; mechanical and hydraulic properties on organic soils were not investigated
Gao *et al.* (2025)	Soft soil	XG	1.5%	UCS = 376 kPa (28 days); 24% UCS drop after 10 wet–dry cycles; Es = 37.1 MPa	Investigated mechanical durability but only on inorganic soft soil
Baghdir *et al.* (2024)	Desert sand	XG + PP fibre	2% XG	UCS improved; fibers enhanced ductility; SEM confirmed matrix reinforcement	Focused on sand; no organic matter present
Zhang *et al.* (2024)	Low liquid limit silty soil	XG	2%	UCS up to 6077 kPa; permeability ↓ 98.9% at 0.75%; improved disintegration resistance	Strong mechanical gains but tested only on silty soils
Hamza *et al.* (2023)	Expansive soil	XG	1.5%	UCS and CBR improved	No evaluation of hydraulic response or organic-rich soils
Kumara and Sujatha (2020)	Clayey sand	β-glucan	–	Strength improvement	Limited to inorganic clayey sand

have a carbon-capture effect during the production stage, resulting in a minimal carbon dioxide trail and thus frequently categorized as sustainable, carbon-neutral, and eco-friendly additives (Chang *et al*. 2016, Lee *et al*. 2019). These are now widely used as stabilizers, thickeners, and rheological modifiers in the field of medicine, agriculture, petroleum industry to direct oil flow (Lappin-Scott *et al*. 1988, MacLeod *et al*. 1988), chemical industry, food industry (Chang and Cho 2014), in the development of the shield for zonal remediation (Park and Yen 1994, Perkins *et al.* 2000), and the making of novel binders for the construction industry (Chang *et al*. 2015, Chang *et al*. 2015). Biopolymers are employed in the civil engineering field as very effective water retention agents in concrete additives (Ramachandran *et al*. 2001), and also find applications in erosion control, stabilization of contaminated soil (Khachatoorian *et al*. 2003), liquefaction mitigation, soil strengthening, and slope stabilization. These polymers are primarily used in the geo-engineering field to avoid desertification, reduce water infiltration, and slopes protection (Khatami and O'Kelly 2013). Some researchers, however, believe that biopolymers may be used to directly strengthen the soil aggregates rather than triggering bacterial activities in soil and that a homogenous mixture of biopolymers can be created in the soil system to enhance mechanical characteristics (Chang and Cho 2012). But the strengthening efficacy depends on the dosage and type of biopolymer, soil type/composition, aging conditions, and mixing method. Depending on their associated functional groups, biopolymers can effectively bind soil particles, sediments, organic pollutants, and alloys (Knox *et al*. 2010).

Xanthan gum (XG) biopolymer is now the most extensively used anionic biopolymer for generating biodegradable polysaccharides (Petri 2015), which are synthesized by *Xanthomonas campestris* bacteria using carbohydrate as the major raw source. It is inexpensive, non-toxic, water-soluble, odorless, and shows higher stability in temperature, base stability, acid, salt, along with high resistance to enzymatic hydrolysis and oxidation (Rosalam and England 2006). XG can be utilized as additives for geotechnical applications such as soil erosion control (Ham *et al*. 2018), mitigating soil liquefaction, and enclosing a bioremediation zone (Ivanov and Chu 2008). Recently, the researchers used different biopolymer types like XG, guar gum etc. to stabilize weak inorganic soil subgrades (Chang *et al*. 2015, Hamza *et al*. 2023, Onah *et al*. 2022). The results, which included both unconfined compressive strength (UCS) testing and Scanning electron microscopy (SEM) analysis, showed that XG was a long-lasting and efficient stabilizer that substantially enhanced the compressive strength of treated soils.

Although biopolymer-based ground improvement has gained momentum, the evidence base remains focused on inorganic sands and silts or on surface durability/erosion control. Highly organic soils—with their low shear strength, extreme compressibility, and moisture-sensitive matrix—are still underrepresented. As presented in Table 1, prior studies rarely couple strength, elastic modulus (E_{50}), and hydraulic behavior within a single framework, rarely interrogate dosage–aging effects, and only intermittently relate macro-responses to microstructural evolution. Moreover, guidance for practice typically stops short of threshold-based selection, leaving engineers without quantitative tools to define performance windows for specific geotechnical applications. To address these gaps, the present study develops a coherent micro–macro

(a)

(b)

Fig. 1 (a) Google satellite image of the soil sampling location, and (b) Photograph of the actual sampling site

framework for a highly organic soil treated with XG biopolymer across 0–5% dosage and 0–60 days aging, integrating Standard/Modified Proctor compaction, UCS–E_{50} characterization, and permeability measurements with SEM-based microstructural evidence of gel bridging and pore refinement. The mechanical test results are formalized through performance modeling and threshold-based decision mapping, using application-oriented criteria (e.g., UCS=360 kPa, E_{50}=20,000 kPa, permeability (k)≤10^{-6} cm/s) and a Composite Performance Index (CPI) metric to identify application-specific performance windows rather than universal optima. To support reproducibility and field transfer, the work also documents pH/viscosity of working slurries and a high-viscosity mixing protocol that clarifies practical uniformity limits at higher dosages. Collectively, the study advances the state of practice by quantifying strength–stiffness–hydraulic improvements in an organic geomaterial, explaining their microstructural origins, and operationalizing the findings into decision maps that can directly inform dosage–aging selection in design.

A low-dosage XG binder can meet practical performance targets in highly organic soils: around 1% XG lifts strength–stiffness to UCS ≥ 360 kPa and E_{50} ≥ 20,000 kPa within ~14–28 days of aging, while permeability drops toward $k \leq 1\times10^{-6}$ cm/s by ~28–60 days depending on compaction/moisture. The most efficient dosage–aging window observed is 0.5–1.5% XG with ~14–28 days aging, with ~1% @ ~28 days giving the best balance of mechanical gain and hydraulic resistance. Mechanistically, XG forms gel bridges and a thin viscoelastic film that refines pore throats and densifies contact networks, explaining concurrent stiffness gains and k-reduction. Importantly, this is biopolymer stabilization (instant physicochemical binding, pH-neutral, field-ready), not bioremediation (microbial mineralization), making it faster and easier to deploy for organic subgrades.

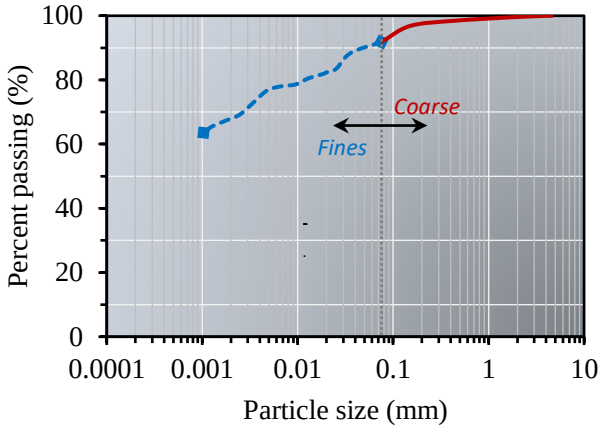

Fig. 2 Gradation curve for untreated organic soil sample

2. Materials and methods

2.1 Test materials

Highly organic soil was collected at a depth of 3–4.5 m below the ground level from Lahore, Punjab, Pakistan. Fig. 1 presents the geographical location and the actual view of the soil sampling site. To minimize alteration of organics, the bulk sample was first air/sun-dried and gently disaggregated; material used for index testing was then low-temperature oven-dried at ~60 °C. Where a higher temperature was required by a specific procedure (e.g., ASTM D4318), we state 105 ± 5 °C explicitly at the point of use and discuss implications in the text. For tests requiring a fines fraction, the soil was lightly pulverized by hand and passed through ASTM No. 200 (75 µm) sieve. Organic content was determined by ASTM D2974 (*LOI*) and was 93% (Table 2). The grain-size distribution is shown in Fig. 2, and the physio-chemical properties are summarized in Table 2.

Specific gravity (Gs) was not measured directly after treatment, as hydrated XG tends to dissolve or adsorb water,

Table 2 Physical and chemical properties of untreated organic soil

Property	Unit	Value
Specific gravity (Gs)	–	1.58
Natural moisture content	%	164
Fiber content	%	76
Organic content	%	93
Void ratio (e)	–	13
Bulk density (γ_{bulk})	kN/m^3	11.2
External surface area	m^2/g	59
SiO_2	%	33
Al_2O_3	%	25
CO_2	%	35
Fe_2O_3	%	5.8
K_2O	%	1.2

Note: The void ratio (e = 13) was measured on undisturbed fibrous organic soil (volumetric method), while bulk density (11.2 kN/m³) refers to the remolded state prepared for laboratory testing

Table 3 Physicochemical properties of pure XG

Property	Unit	Value/Description
Form	–	Yellowish powder
Viscosity	mPa·s	1555
Molecular weight	g/mol	242
Dominant element	–	Calcium

biasing pycnometer readings. Instead, a rule-of-mixtures estimate was used to demonstrate that the effect of XG addition (up to 1–2%) on the apparent Gs is negligible, with a maximum change of ≤0.02. As an alternative, bulk density and void ratio values were reported to provide a more accurate understanding of the material behavior. Furthermore, to highlight the sensitivity of organic soils, the liquid limit (LL) was determined under two preconditioning routes: sun-dried and low-temperature oven-dried (~60°C), following ASTM D4318. The LL of the sun-dried soil was 115%, while the LL of the oven-dried soil decreased to 90%, indicating a reduction of about 22%. This decrease is consistent with previous reports on organic soils, where oven heating removes bound water and alters humic matter, thereby reducing water-holding capacity (Basma *et al*. 1994). Such differences confirm the organic nature of the soil and emphasize the need for caution when comparing Atterberg limits obtained under different drying regimes.

XG biopolymer, a polysaccharide used primarily as a food additive and rheology adjuster, is made by fermenting glucose or sucrose with the bacteria *Xanthomonas campestris*. The pyruvylated mannose, D-mannose, 6-O-acetyl D-mannose, D-uronic acid, and 1, 4-linked glucan from the anionic polysaccharide that results (Cadmus *et al*. 1982). XG has a linear linked b-D glucose backbone with a trisaccharide side chain connected to each glucose in its chemical structure. Unlike other biopolymers, XG is more stable across a wide range of temperatures and pH (Zohuriaan and Shokrolahi 2004). XG has long been used in the oil industry as a drilling mud thickening to maintain consistent rheology throughout the drilling hole. It's also been utilized as a concrete additive to improve viscosity and prevent washouts (Comba and Sethi 2009). The physiochemical properties of pure XG are tabulated in Table 3.

The physical form and SEM micrographs of test materials are presented in Fig. 3. The SEM micrographs reveal distinct structural differences between the two materials: the soil sample shows a rough and granular surface with larger, irregular particles, characteristic of untreated soil, while the XG sample exhibits a smooth, amorphous surface with a porous and clustered texture, typical of biopolymer materials. This structure suggests that XG particles can fill soil voids and enhance stability by bonding with soil particles. Also, the EDX analysis further supports these observations. The soil sample is dominated by oxygen (O) and silicon (S), confirming its silica-rich composition. In contrast, the XG sample primarily contains carbon (C) and oxygen (O), reflecting its biopolymeric nature, with smaller amounts of aluminum (Al), magnesium

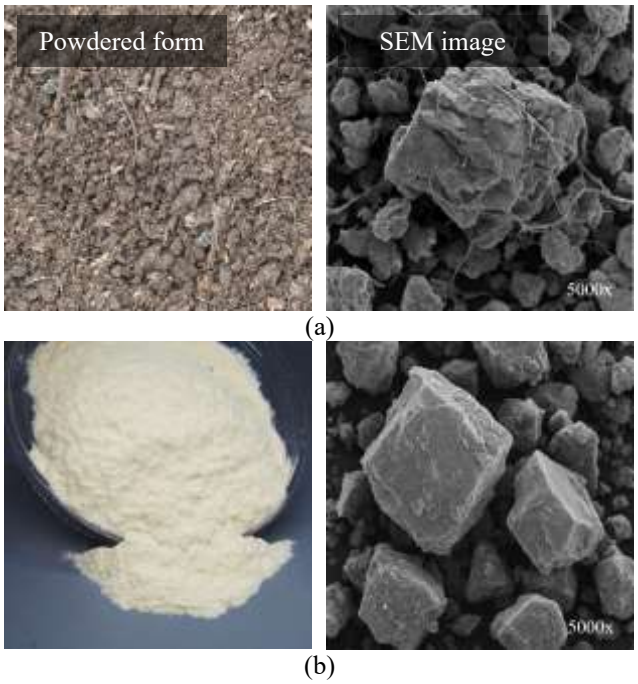

Fig. 3 Powdered form and SEM micrograph of (a) untreated organic soil, and (b) XG powder

Table 4 Properties of biopolymer mixing slurry at 25°C

Dosage (%)	pH (25 °C)	Apparent viscosity (mPa·s)	Practical note
0.5	6.3–6.8	600–800	Easy to spray-mix; shear-thinning
1.0	6.3–6.8	1,200–1,600	Useful hydration check
2.0	6.3–6.8	3,000–4,000	Thick; mixable with staged water and a planetary mixer; near practical limit

(Mg), iron (Fe), potassium (K), calcium (Ca), and sodium (Na) present as trace elements. These results indicate that the interaction between the XG's carbon and oxygen and the soil's silicon and oxygen can facilitate soil stabilization, improve its mechanical properties and contribute to enhanced soil structure.

2.2 Soil sample preparation and testing

Working biopolymer slurries were prepared at 0.5, 1.0, and 2.0% (w/v) and equilibrated at 25°C before use. The pH at 25°C was near-neutral (≈6.3–6.8), consistent with the broad stability reported for natural-polymer solutions (e.g., Katzbauer (1998). Apparent viscosity (Brookfield LV, 25 °C; spindle/rpm per instrument range) was about 600–800 mPa·s at 0.5%, 1,200–1,600 mPa·s at 1.0%, and 3,000–4,000 mPa·s at 2.0% (Table 4), in line with the known shear-thinning, concentration-dependent rheology of xanthan-type biopolymers (Casas *et al*. 2000, Zohuriaan *et al.* 2004). Guided by these checks, the biopolymer was pre-hydrated as 1–2% slurries using an overhead stirrer (≈300–500 rpm, 30 min) and rested 12 h for full hydration; slurries were then spray-added while blending soil in a planetary

mixer for 5–8 min with two-stage water addition to prevent clumping. Mixed material was sealed for 24 h at 23 ± 2°C to homogenize moisture ("aging"), and a simple visual homogeneity check (no gel clumps; uniform crumb) was applied. Practical handling limits were noted above ≈2% dosage.

Standard and biopolymer-treated soils were compacted according to ASTM D1557-12e1 to establish OMC and MDD; target molding water contents for strength and hydraulic specimens were taken from the Proctor curves. Cylindrical UCS specimens were molded to 38 mm diameter × 76 mm height in accordance with ASTM D2166/D2166M-16 and conditioned at relative humidity≈70% and 23±2°C prior to testing. Unconfined compression was performed under deformation control at 0.8 mm/min to obtain stress–strain response and E_{50} from the primary loading branch. Hydraulic conductivity was measured using a flexible-wall permeameter following ASTM D5084, with specimen saturation by back-pressure to standard acceptance and tests conducted at the designated confining stress within the method's gradient limits.

CPI was calculated for each dosage–aging–compaction energy combination using Eqs. (1) and (2). For each treated case, the baseline (UCS_0, $E_{50,0}$, k_0) was taken from the untreated (0% XG) specimen at the same compaction energy (Standard or Modified) and the same aging day; where an exact untreated age was unavailable, the baseline was obtained by linearly interpolating between the two nearest untreated ages. The mechanical CPI (Eq. (1)) is reported as the primary metric; the hydraulic-inclusive CPI (Eq. (2)) serves as a sensitivity analysis with w_h = 0.25, and the permeability term is treated on a benefit-inverted basis, i.e., $(k_0 - k)/k_0$. All terms were non-dimensionalized by their respective untreated baseline values to eliminate unit effects.

Data integrity checks included: (i) recomputing CPI directly from the raw UCS, E_{50}, and permeability data; (ii) Pearson correlations showing positive association between CPI and UCS/E_{50}, and a negative association with $\log_{10}(k)$; and (iii) a parsimonious regression model, CPI ~ dosage + age + (dosage × age). Due to the small sample size, leave-one-out cross-validation (LOOCV) was used with RMSE as the stability metric, and R^2 was also reported for transparency. Uncertainty was quantified using bootstrap (1,000 resamples) to obtain 95% confidence intervals for slopes and fit statistics. All CPI values were consistent with corrected compaction parameters and remain physically coherent with the zero-air-voids constraint for Gs = 1.58.

$$\text{CPI}\ (\%) = \frac{1}{2}\left(\frac{\text{UCS}-\text{UCS}_0}{\text{UCS}_0} + \frac{E_{50}-E_{50,0}}{E_{50,0}}\right) \times 100 \qquad (1)$$

$$\text{CPI}_h\ (\%) = \frac{1}{2}\left(\frac{\text{UCS}-\text{UCS}_0}{\text{UCS}_0} + \frac{E_{50}-E_{50,0}}{E_{50,0}}\right) \times 100 + w_h\left(\frac{k_0-k}{k_0}\right) \times 100] \qquad (2)$$

where:

- CPI: Measures the improvement in mechanical properties (strength and stiffness) only
- CPI_h: Measures the improvement in mechanical properties and includes a term for permeability, with the weighting factor w_h (usually set to 0.25)
- UCS, E_{50} , k = strength, stiffness, and permeability of treated soil
- UCS_0, $E_{50,0}$, k_0 = untreated baseline values at the same compaction energy and age
- w_h= hydraulic weighting factor (here w_h= 0.25)

Performance modeling and decision mapping were carried out to translate the mechanical and hydraulic test results into application-oriented guidance. Measured UCS and E_{50} values at different dosages (0–5%) and aging times (0–60 days) were modeled using ordinary least squares (OLS) with linear, power, and logarithmic fits; model accuracy was evaluated using R^2, RMSE, and 5-fold cross-validation. To visualize performance domains, the discrete test data were interpolated onto a regular dosage–aging grid using bivariate cubic interpolation (*SciPy*, *Python 3.9*). From these interpolated surfaces, decision maps were constructed based on thresholds commonly cited for subgrade performance: UCS ≥ 360 kPa, E_{50} ≥ 20,000 kPa, and a CPI ≥ 200%. These maps delineate performance windows where the criteria are simultaneously satisfied, rather than prescribing a single "optimum," thereby offering practical ranges of dosage and aging that can be adapted for different geotechnical applications.

3. Results and discussion

3.1 Impact of XG stabilization on compaction behavior of organic soils

The effect of XG on optimum moisture content (OMC) and maximum dry density (MDD) from Standard and Modified Proctor tests is shown in Fig. 4(a). Consistent with compaction theory, dry density increases with water content up to an optimum and then decreases. The higher Modified Proctor energy (≈2695 kJ/m³) produces higher MDDs and slightly lower OMCs than the Standard Proctor test (≈593 kJ/m³). The Standard Proctor series shows MDD decreasing from 8.9 to 7.4 kN/m³ as XG rises from 0% to 5% (≈17% reduction), accompanied by OMC increasing from 25% to 40% (≈60% increase). The Modified Proctor series exhibits the same trend, with MDD decreasing from 9.5 to 8.0 kN/m³ (≈16% reduction) and OMC increasing from 23% to 38% (≈65% increase). These changes reflect XG's gel-water demand and lower solid density, which shift the compaction optimum to higher moisture while slightly reducing achievable dry unit weight; all reported MDD values remain below the Zero Air Void (ZAV) envelope, as illustrated in the inset.

For broader context, Fig. 4(b) compares the compaction characteristics of the XG-treated organic soil with those reported for cement-, lime-, and biopolymer-treated inorganic soils (Barman and Dash 2022, Dehghan *et al.* 2019, Peethamparan and Olek 2008). Cement-stabilized soils typically achieve MDD in the range of 15–19 kN/m³ at OMC of 12–18%, while lime-treated soils yield 15–18 kN/m³ and 15–22%, respectively. Biopolymer-treated inorganic soils generally exhibit 14–17 kN/m³ MDD and

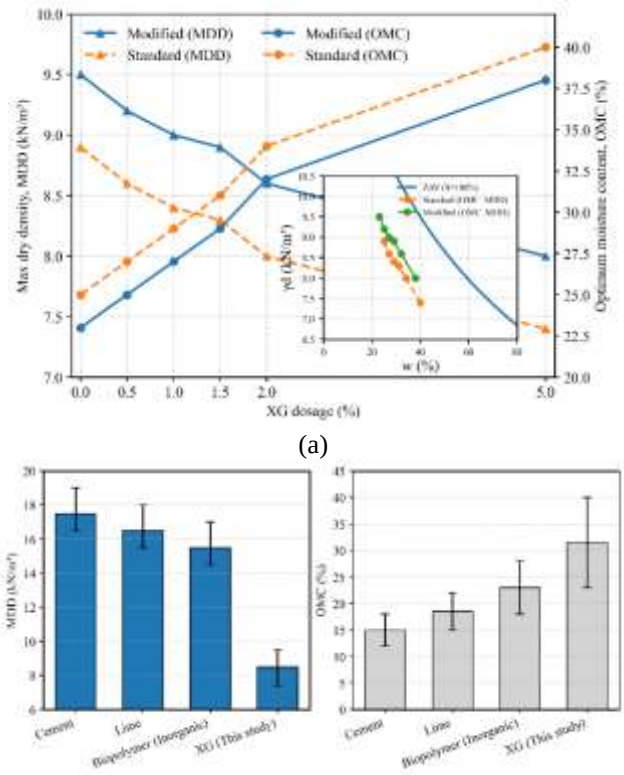

Fig. 4 (a) Compaction behavior of XG-treated soil under Standard and Modified Proctor energies, and (b) Literature-based comparison of compaction characteristics for various stabilizers versus XG-treated soil

18–28% OMC. In contrast, the highly organic soil investigated in this study shows a markedly lower MDD of 7.4–9.5 kN/m³ and a higher OMC of 23–40%, consistent with its low specific gravity (Gs = 1.58) and the gel-water demand of XG. This comparison underscores that while cement and lime increase density and reduce moisture demand, biopolymer treatment—especially in organic soils—favors water retention and slightly reduces compacted density.

In both Standard (ASTM D698) and Modified (ASTM D1557) Proctor tests, the MDD decreases with increasing biopolymer content because part of the mineral skeleton is replaced by a low–specific-gravity, irregular, porous polymer phase, and the formation of hydrated gel films occupies volume and disrupts dense packing. In parallel, the OMC increases with dosage because the polymer is strongly hydrophilic and has a high specific surface area/internal porosity; water is partitioned between (i) pore water that contributes to densification and (ii) bound water in the polymer network that does not aid compaction, so more water is required to reach the target state. Comparing compactive energies, the higher effort of the Modified Proctor collapses macro-voids and expels air more effectively, yielding higher MDD and lower OMC than the Standard Proctor at the same dosage; however, the upward OMC shift with increasing dosage persists under both energies because of the polymer's water demand. At higher contents (≈≥2%), viscous gel formation can further limit particle rearrangement and marginally accentuate the MDD drop. These trends agree with prior studies on biopolymer-treated fine-grained soils, which consistently reported decreasing MDD and increasing OMC with dosage (Chen *et al.* 2019, Latifi *et al.* 2017).

3.2 Enhancing shear strength of organic soils with XG stabilization

The soil structure treated with stabilizers gradually evolves with time due to continuous gelation reactions; therefore, strength-time development is crucial in studying the strength properties of such soils (Peethamparan and Olek 2008). To demonstrate the strength and cohesion development with time for organic soil ameliorated with XG, the stress-strain response was recorded for each blend, cured for 4, 7, 14, 28, and 60 days to develop the stress-strain curves shown in Fig. 5. All the soil samples were prepared using standard compaction results. The aging period refers to the time between the point of making the mold and finally testing it.

The peak stress (q_u) and undrained shear strength (c_u) of mixtures amended with 1% XG and cured for 7 days reached a peak value of 275 and 138 kPa, respectively, at a strain of about 4.6%, while the mixtures of the same composition cured for 28 and 60 days attained a peak stress of 554 and 698 kPa and cohesion of 277 and 349 kPa at a strain of 3.7 and 2.4% respectively. Thus, it represents a 19.6 and 47.8% decrease in the strain at failure compared to a mixture cured for 7 days. Similar behavior has been observed for other XG percentages. When observing the stress-strain behavior of the soil blends tested directly after their preparation, a relatively ductile behavior was noticed due to the continuous and gradual deformation of mixtures until peak stress was reached. But the stress-strain curves of XG-treated samples exhibit a leftward shift, indicating an increase in stiffness and a reduction in failure strain with increased aging periods. Hence, these mixtures became stiffer with time due to continued gelation reaction in the soil system and consequently achieved the peak stress value at a much smaller strain.

3.2.1 Unveiling the mechanisms of soil-XG interaction and strength enhancement

Fig. 6 depicts the method of interaction between the XG and soil particles present in the organic soil matrix. The mechanical properties of soil, such as shear strength, deformation characteristics, permeability, and expansion potential, are influenced by its structure. Isomorphic substitution, in general, stimulates the detachment of hydroxyl ions (OH^-) from the soil's surface, resulting in an electrical imbalance. This electrical imbalance generally upsurges cations and water particles (Kumar *et al.* 2021). Water is a dipolar atom, which possesses one negative and one positive charge. The negatively charged soil surface attracts and creates hydrogen bonds with the positively charged H^+ ions in the water. The bond formation is determined by the type of clay minerals used. If the attraction of molecules in the soil grains is strong, their plasticity increases, and their strength characteristics are

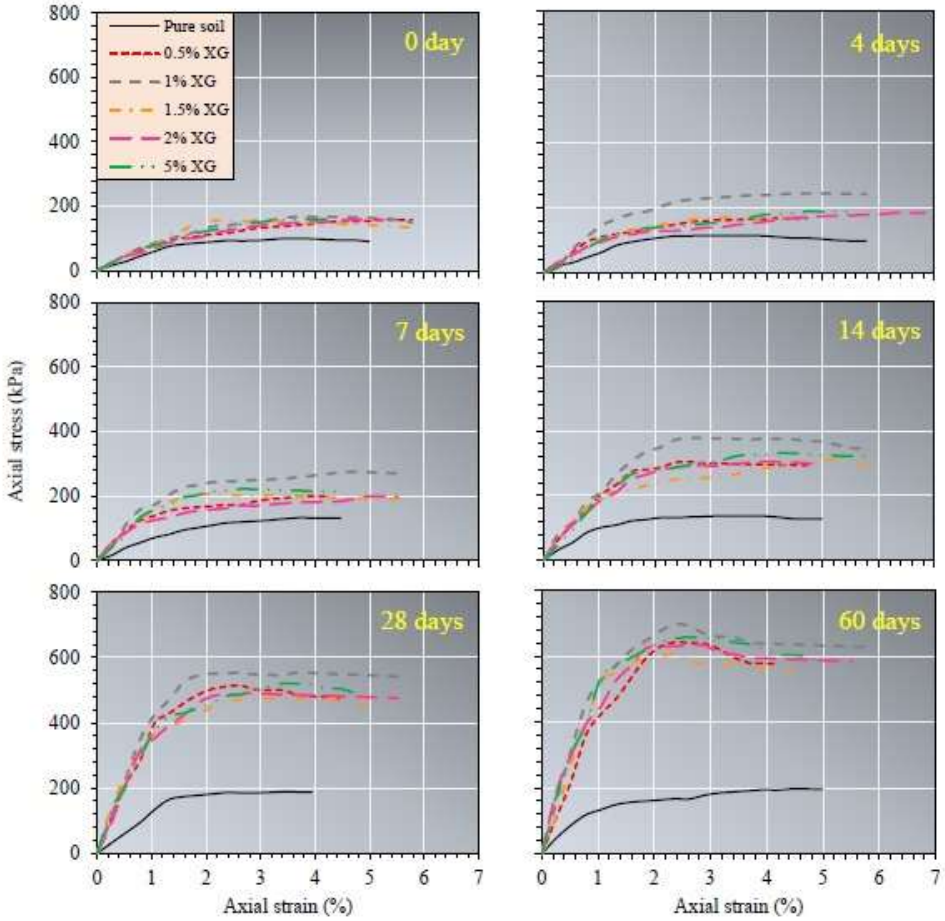

Fig. 5 Stress-strain behavior of soil samples in UCS tests at different aging days (0 to 60 days)

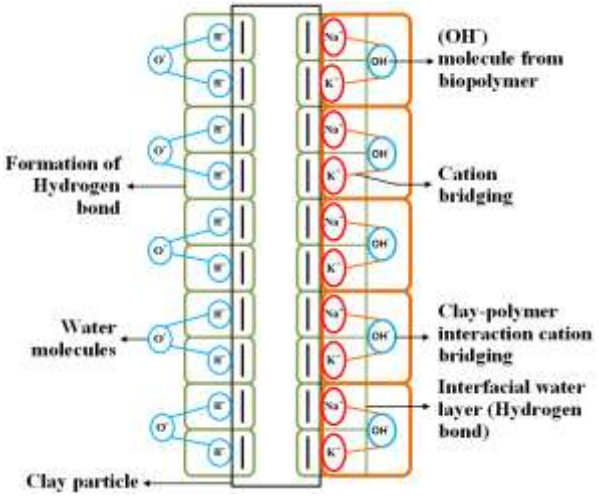

Fig. 6 Mechanism of soil–XG and water interaction (modified from Latifi *et al.* 2016)

considerably altered. Because of their negatively charged surfaces, clay particles will adsorb water molecules in voids of soil particles. These cations form double layers as they spread across the surface of the clay particles.

Because of K^+ and Na^+ ions in the pore solutions, the cation exchange sites on the clay surfaces are filled. The interfacial water layer formed by K^+ and Na^+ ions around the clay particles limits the ability of XG to establish hydrogen bonds with the clay particles. XG, while being non-ionic, has many hydroxyl molecules. Thus, hydroxyl molecules in the XG are absorbed by soil cations and create a clay polymer relationship via cation bridging. The strength of the XG-treated mix increases as the amount of XG absorbed by clay particles increases.

The formation of biopolymer hydrogels responsible for the observed strength enhancement in XG-stabilized soils is visually depicted in Fig. 7. Fig. 7(a) presents SEM micrographs of soil stabilized with 1% XG biopolymer at different aging times (from 0 to 60 days). The micrographs clearly illustrate the initial stage of gel formation, where a relatively sparse network of XG gel bridges connects the soil particles. This early-stage interaction results in a looser and more porous soil structure with fewer gel bridges between particles (from 0 to 7 days). And this bridge-like structure becomes more developed and hardened with aging up to 60 days, binding the soil particles together to make a hardened soil fabric.

Fig. 7(b) presents the proposed interaction mechanism as observed in the scanning electron micrograph. Over the time, as the soil continues to age, the XG biopolymer undergoes further gelation, creating a denser network of gel

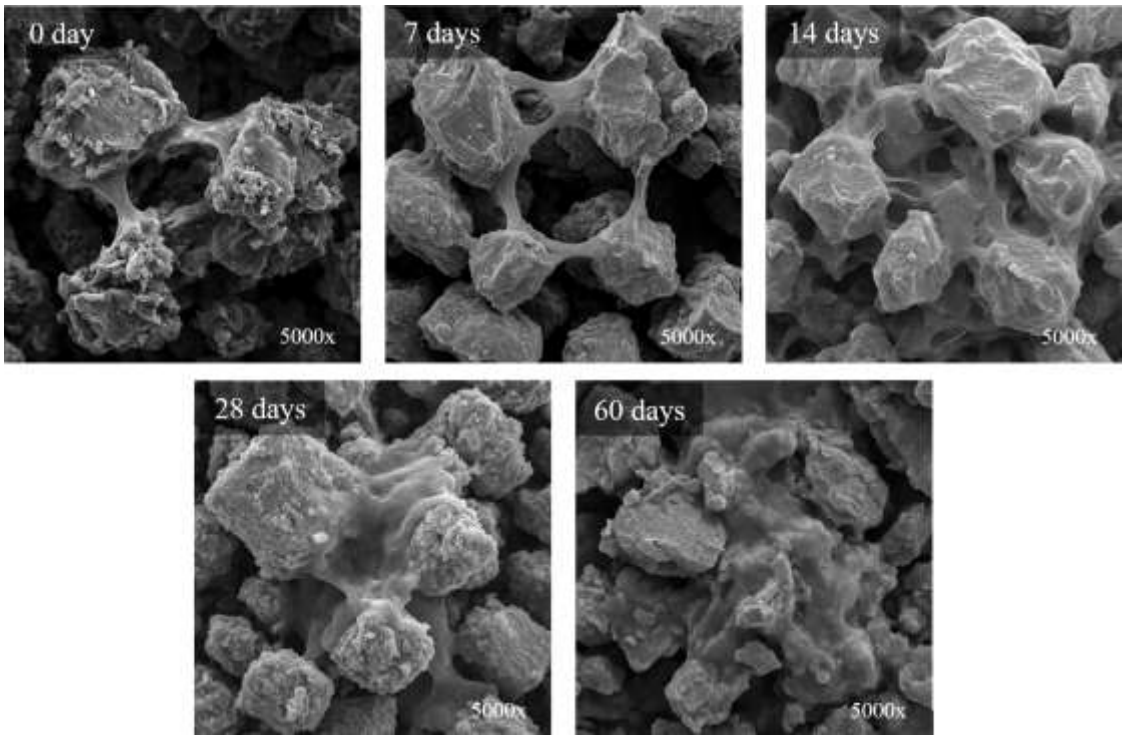

(a)

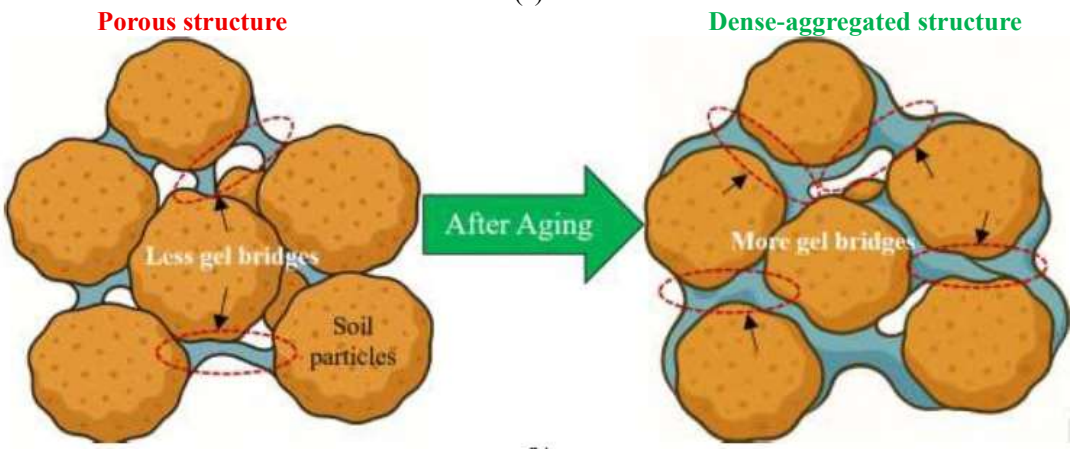

(b)

Fig. 7 (a) SEM micrographs of 1% XG-treated soil at different aging times, and (b) proposed Soil-XG interaction mechanism based on scanning electron micrographs

bridges between soil particles (Ayeldeen *et al*. 2017). This progression leads to a more cohesive and compact soil matrix, enhancing the overall strength and stability. The increased gel bridging effectively reduces the void spaces within the soil, providing improved resistance to deformation under load, which is consistent with the observed increase in UCS and reduced permeability in the XG-treated soils. This aging-dependent microstructural evolution highlights the long-term strengthening effect of XG biopolymer, making it an effective stabilizer for highly organic soils.

3.2.2 Influence of aging on UCS and E_{50} strength development

The effect of XG content was most pronounced in the soil specimens amended with 1% XG, which demonstrated the highest UCS strength value up to 60 days of the aging period, as shown in Fig. 8(a). According to Das and Sobhan (2013), the sample treated with 1% XG was transformed from low to hard quality subgrade *(UCS ≥ 360 kPa)* when the aging period reached 28 days. The UCS strength of soil samples amended with 5% XG content was the next strongest, while the samples amended with remaining XG contents exhibited the lower strength. It may be due to unreacted XG particles, the formation of micro-cracks in the soil structure, and the increased replacement of clay particles by porous & lightweight XG particles. Likewise, the elastic modulus of soil also shows considerable enhancement of stiffness with the aging process up to 60 days, as shown in Fig. 8b, and the low-quality subgrade also transforms to a hard subgrade *(E_{50} ≥ 20,000 kPa)* based on the requirement proposed by the researcher (Obrzud 2010).

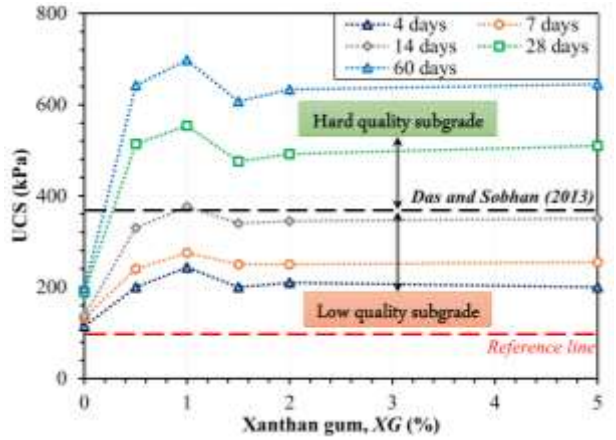

(a)

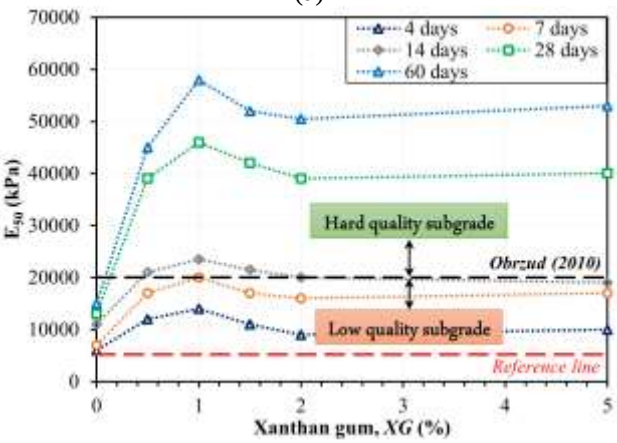

(b)

Fig. 8 (a) UCS vs. dosage/aging with target band UCS≈360 kPa (Das and Sobhan 2013), and (b) E_{50} vs. dosage/aging with target band E_{50}≈20,000 kPa (Obrzud 2010)

The combination of XG with soil particles develops a stiff soil-biopolymer matrix with a flocculated structure; this matrix differs from untreated natural soil in terms of reduced pore spaces and improved stiffness (Ivanov and Chu 2008).

Subgrade suitability was assessed using measured metrics—UCS and E_{50}—rather than CBR, which was not part of this test program. Across dosage and aging, mixtures that reached UCS ≥ 360 kPa and E_{50} ≥ 20,000 kPa are highlighted as meeting typical subgrade quality targets. These mechanics-based thresholds align with strength- and modulus-oriented guidance reported in the literature and avoid inference from unmeasured CBR values. The resulting performance windows (Fig. 8) show that ≈1% biopolymer within 14–28 days consistently meets both criteria, with diminishing gains at higher dosages due to mixing/viscosity constraints.

To holistically assess the improvement in mechanical behavior, a CPI was formulated by averaging the percentage increase in UCS and elastic modulus relative to the untreated soil. The resulting CPI values at 28 and 60 aging days are shown in Fig. 9. The CPI trend confirms that 1% XG achieves the highest overall enhancement, with a peak CPI of 308.7% at 60 days. While 1.5%, 2%, and 5%

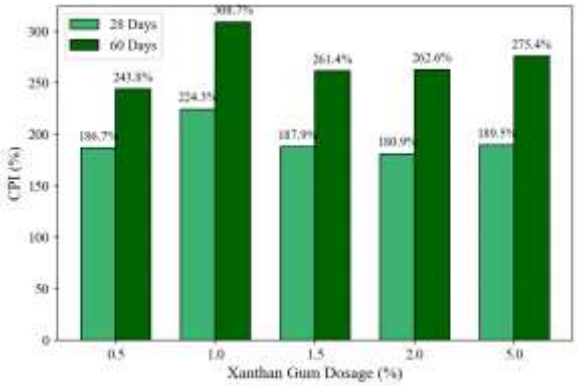

Fig. 9 Composite Performance Index for UCS and E_{50} at 28 and 60 days of aging for various XG dosages

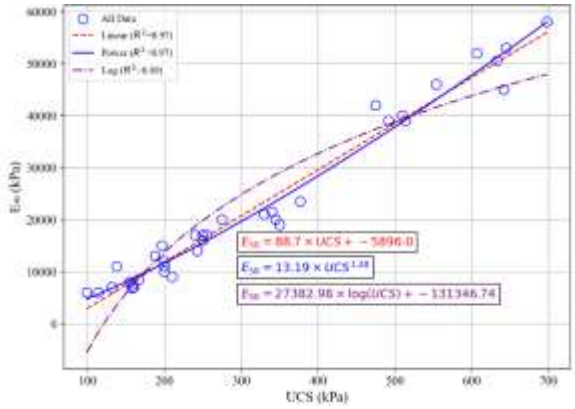

Fig. 10 Correlation between UCS and E_{50} with fitted linear, power, and logarithmic models

dosages also demonstrate high performance, the gain beyond 1% becomes relatively marginal (e.g., 275.4% at 5% vs. 308.7% at 1%). These diminishing returns, when considered alongside higher material demand and potential workability issues, further justify 1% as the optimal dosage. Notably, 0.5% XG shows significant improvement at early aging stages but is consistently outperformed by higher dosages as the aging progresses. These CPI results support earlier strength and stiffness findings and reinforce the recommendation of 1% XG as a cost-effective and technically balanced stabilizer for highly organic soils.

3.2.3 Performance modeling and decision mapping for threshold optimization

Having established the strength and stiffness gains, the results were synthesized into performance models to provide practical design guidance. To evaluate the performance dynamics of XG-stabilized organic soil, both regression modeling and threshold-based decision maps were developed (Figs. 10 and 11). Fig. 10 illustrates the empirical relationship between UCS and E_{50} using linear, power, and logarithmic fits. All models demonstrate a strong correlation (R^2≈0.97), indicating that E_{50} can be reliably predicted from UCS. The power model shows slightly better fit across the range, consistent with the nonlinear growth behavior typically seen in biopolymer-treated systems.

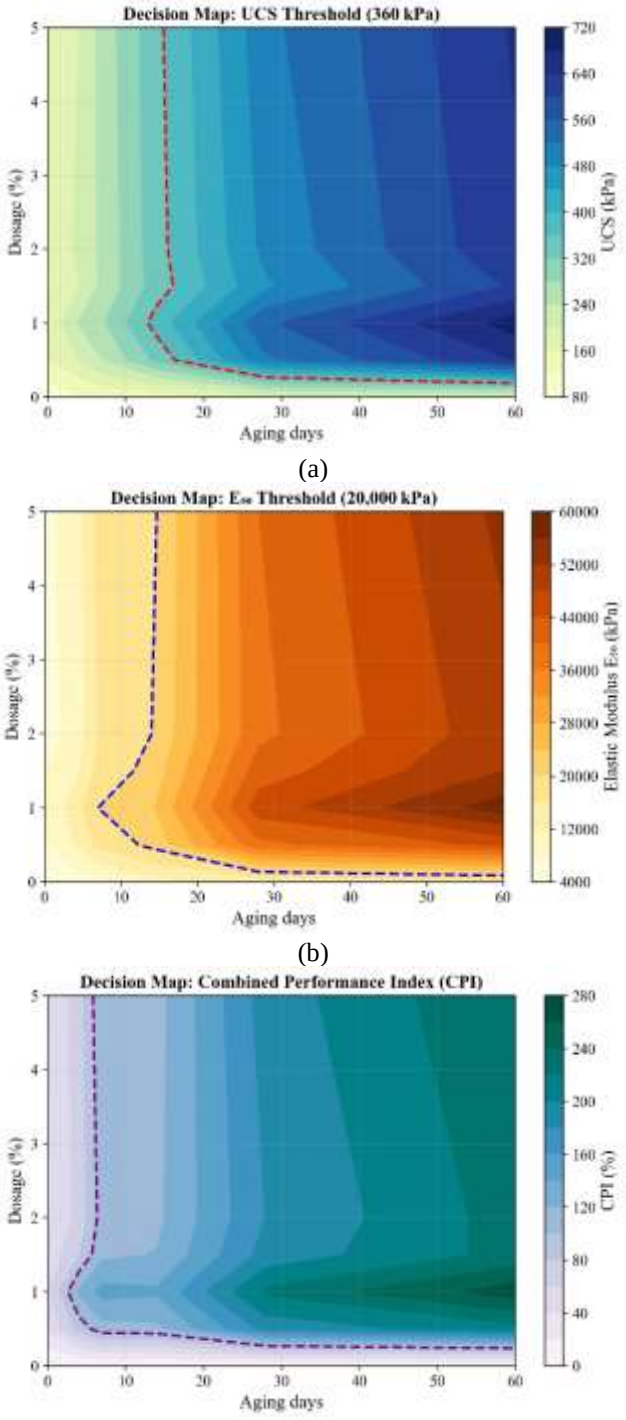

Fig. 11 Decision maps for XG-treated organic soil: (a) UCS with 360 kPa threshold, (b) E_{s0} with 20,000 kPa threshold, and (c) CPI highlighting application-specific performance windows

To guide practical dosage and aging recommendations, decision maps were generated using contour plotting. Fig. 11(a) presents the UCS decision map with a red dashed contour marking the 360 kPa threshold. It is evident that 1% XG achieves this criterion by 14–28 aging days, whereas higher dosages meet the same target sooner, but with diminishing performance gain relative to material cost. Similarly, Fig. 11(b) shows the E_{s0} decision map with a 20,000 kPa threshold delineated in blue. The results confirm that 1% XG again reaches the design stiffness zone after 14 days, supporting its suitability for applications requiring moderate to high stiffness. While 1.5%–5% dosages offer faster or slightly higher gains, the improvement is marginal relative to increased material use. Finally, Fig. 11(c) presents the CPI, integrating both UCS and E_{s0} improvements. The CPI map confirms that the 1% XG dosage falls within the high-performance envelope across aging time. The threshold line (≥200%) encapsulates the same region identified by the previous two criteria, reinforcing 1% as the most efficient and structurally balanced dosage.

These plots collectively support the selection of 1% XG as the optimum stabilizer dosage, achieving target mechanical thresholds with aging periods as short as 14–28 days. The convergence of all three performance indicators at this dosage makes it a strong candidate for field-scale implementation.

3.3 Evolution of permeability in XG-stabilized organic soils

Fig. 12 presents the permeability behavior of XG-stabilized organic soil as a function of dosage and aging time. A sharp reduction in permeability was observed with increasing XG content and aging period. As shown in Fig. 12(a), adding just 1% XG led to a reduction of approximately three orders of magnitude, while 5% XG achieved a decrease of nearly five orders of magnitude relative to untreated soil. This remarkable decline is attributed to the development of highly viscous hydrogels that fill voids and effectively clog pore pathways, consistent with findings by Bouazza *et al.* (2009) and Dehghan *et al.* (2019). The permeability continued to decrease over time for all treated samples, suggesting that hydrogel consolidation, crosslinking interactions, and progressive pore obstruction remain active during aging. The log-scale heatmap in Fig. 12(b) further visualizes this downward trend in permeability with clear dosage–time zones of optimal sealing performance. To provide a comprehensive performance perspective, Fig. 12(c) overlays permeability contours with CPI thresholds. The red dashed line marks the permeability criterion of 1×10^{-6} cm/s, while magenta dashed lines denote CPI zones of 150% and 250%. The intersection of these thresholds highlights a clear optimum performance zone at 1% XG and 28–60 days aging, offering the best trade-off between permeability control and mechanical efficiency.

The shaded region in the decision maps is not a single global "optimum," but an application-specific performance window defined by the adopted subgrade criteria (UCS ≥ 360 kPa, E_{s0} ≥ 20,000 kPa, $k \leq 1\times10^{-6}$ cm/s, and CPI ≥ 200%). Within this window—typically around ≈1% biopolymer and ≈14–28 days—the measured strength–stiffness–hydraulic responses are simultaneously satisfied. For other applications (e.g., liners or seepage control with stricter k, or bases demanding higher E_{s0}), the same mapping framework applies by simply adjusting the thresholds.

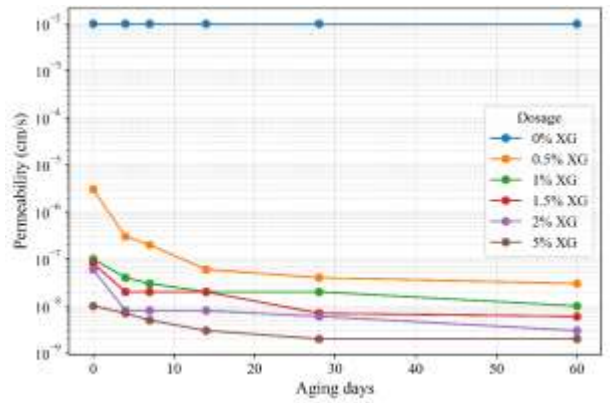

(a)

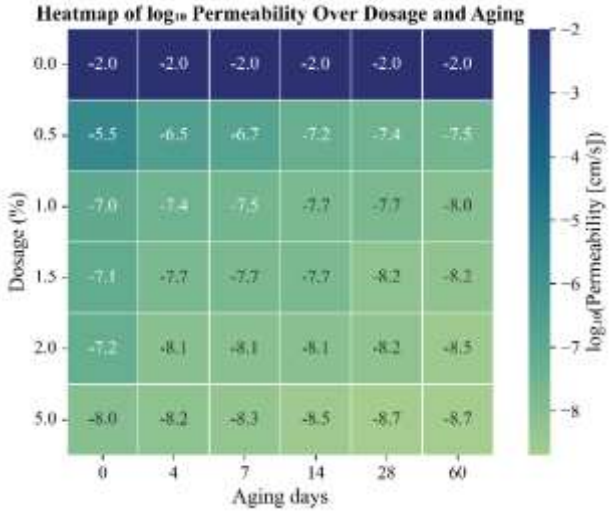

(b)

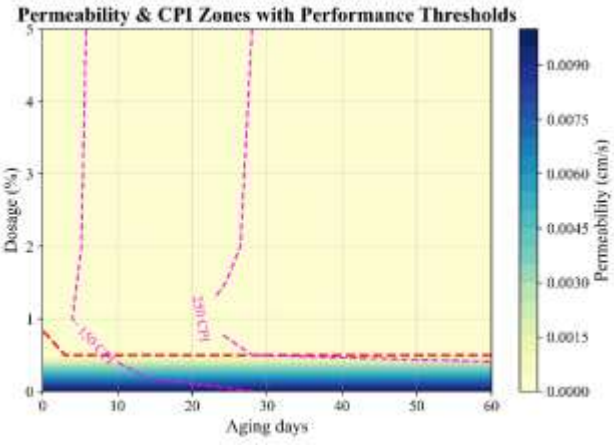

(c)

Fig. 12 (a) Hydraulic conductivity ($\log_{10}k$) versus aging for various biopolymer dosages, (b) Dosage–aging heatmap of $\log_{10}k$, and (c) Contour map showing the performance window where $k \leq 1\times10^{-6}$ cm/s and CPI ≥ 200% are met

The microstructural changes in XG-treated soils, as shown in Fig. 13, provide insight into the observed reduction in permeability with increasing aging time. At 0-day aging (Fig. 13(a)), the SEM micrograph reveals the presence of voids and irregular gaps within the soil matrix, even with 1% XG treatment. These initial gaps represent a porous structure that would normally allow for relatively high permeability. As the aging period progresses, particularly after 28 days (Fig. 13(b)), the SEM image clearly shows that these voids are progressively filled with dense, gel-like biopolymer formations. The biopolymer matrix effectively bonds soil particles together, leading to a significant densification of the soil structure. The gelation of the XG creates a more cohesive network that constricts pore spaces and blocks the movement of water through the soil.

This transition from a more open to a highly compacted structure supports the hypothesis that the XG-induced gelation is the primary mechanism driving the observed reduction in permeability. The pore clogging effect, which intensifies with aging, significantly impedes the flow paths for water, resulting in a drastic decrease in hydraulic conductivity. This behavior is consistent across all XG dosages, with the most notable effect occurring as the soil continues to mature over time. These microstructural observations provide compelling evidence for the role of XG in creating a highly impermeable barrier through the development of a stable, gelled matrix that strengthens over time, reducing permeability by over three orders of magnitude after 28 days of aging.

4. Environmental impact and sustainability of XG-based soil stabilization

XG presents a sustainable alternative to traditional stabilizers like cement, which accounts for ~5% of global CO_2 emissions (Andrew 2018, Chang *et al*. 2015). In contrast, XG is produced via bacterial fermentation—a low-energy, renewable process—and is biodegradable, non-toxic, and avoids groundwater contamination. Its use transforms problematic organic soils, often deemed waste, into viable construction materials, supporting circular economy principles by reducing disposal needs and virgin material consumption (Cheng and Geng 2023). The significant permeability reduction achieved with XG treatment further enables applications in hydraulic barriers and land reclamation, contributing to water conservation and ecosystem restoration. While a full Life Cycle Assessment (LCA) is recommended for quantitative comparison, XG fundamentally aligns with sustainable geotechnical goals by offering a bio-based, eco-compatible solution that enhances soil properties while minimizing environmental degradation.

5. Limitations and future work

This study's findings are based on laboratory conditions, and their translation to field applications requires further validation. Key limitations that define future research directions include the absence of zeta potential analysis to elucidate electrokinetic interactions, and the need to assess long-term durability under environmental cycles (e.g., wet-dry, freeze-thaw) and biological degradation. Subsequent work should focus on field-scale trials to validate the identified performance windows and a comprehensive LCA

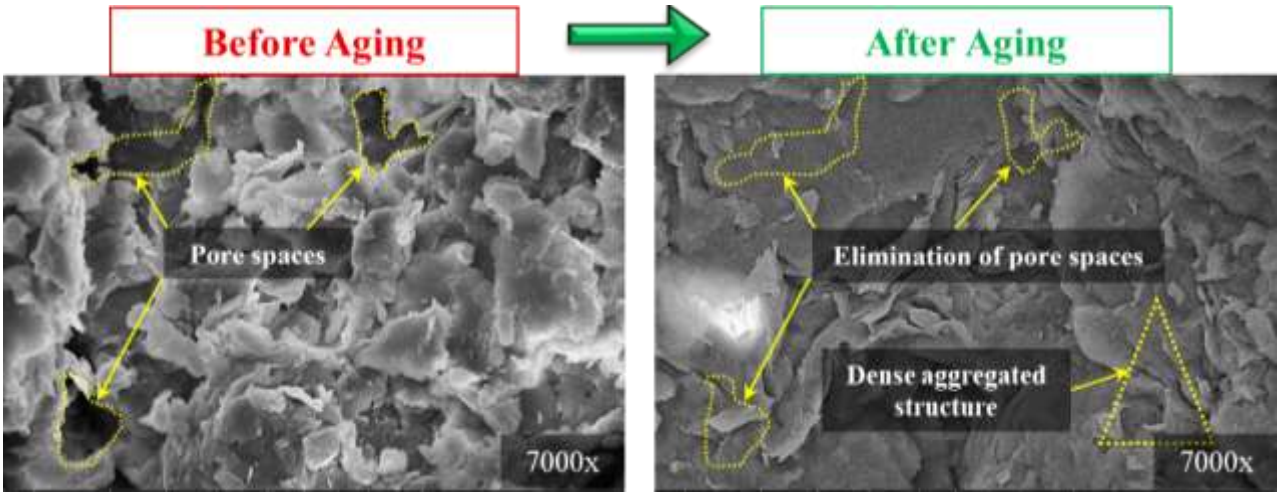

(a) (b)

Fig. 13 SEM micrographs of 1% XG-treated soil: (a) 0-day, and (b) 28-days aging, showing pore clogging and densification

to quantitatively benchmark the environmental benefits of XG against conventional stabilizers. Addressing these points will solidify the practical implementation and sustainability credentials of biopolymer-based stabilization for organic soils.

6. Conclusions

This study evaluated the macro- and micro-scale performance of highly organic soils stabilized with a XG biopolymer. Laboratory testing showed that a dosage of about 1% provides a balanced solution, achieving a sixfold UCS increase (99 to 698 kPa), meeting the $E_{50} \geq 20{,}000$ kPa stiffness criterion within 28 days, and reducing permeability by 3–5 orders of magnitude below the critical 1×10^{-6} cm/s threshold. Decision maps demonstrated that this dosage–aging window represents an application-specific performance range, with higher dosages offering diminishing returns due to viscosity and mixing constraints. Microstructural evidence from SEM confirmed the progressive formation of dense gel matrices and pore filling, supporting the observed durability and low permeability. Collectively, these results indicate that ≈1% biopolymer is sufficient for meeting strength, stiffness, and hydraulic requirements for subgrade stabilization and barrier applications, while also reducing material consumption. From a geotechnical perspective, the combined use of mechanical thresholds (UCS/E_{50}), hydraulic cutoff (k), and CPI provides a reproducible framework for defining performance windows rather than single optima. The scope of this work was limited to laboratory-scale specimens under controlled aging, and future studies should validate these findings under field conditions, cyclic environmental loading, and long-term durability scenarios. Nevertheless, the results underscore the potential of biopolymers as sustainable, cost-effective, and environmentally compatible alternatives to conventional chemical stabilizers, contributing to resilient infrastructure development in organic soil regions. This study establishes XG as a viable, sustainable, and high-performance stabilizer that can transform challenging organic soils into reliable engineering materials.

Acknowledgments

The authors gratefully acknowledge the College of Civil and Transportation Engineering, Shenzhen University, Shenzhen, China, for laboratory facilities, computational resources, and technical support throughout this study. We also thank the geotechnical laboratory staff for their assistance during specimen preparation and testing.

References

ASTM International. (2019), Standard test methods for laboratory determination of water (moisture) content of soil and rock by mass (Standard No. ASTM D2216-19). ASTM International.

ASTM International. (2014), Standard test methods for specific gravity of soil solids by water pycnometer (Standard No. ASTM D854-14). ASTM International.

ASTM International. (2020), Standard test methods for determination of moisture, ash, and organic matter of peat and other organic soils (Standard No. ASTM D2974-20). ASTM International.

ASTM International. (2017), Standard test methods for liquid limit, plastic limit, and plasticity index of soils (Standard No. ASTM D4318-17). ASTM International.

ASTM International. (2012), Standard test methods for laboratory compaction characteristics of soil using standard effort (12,400 ft-lbf/ft³; 600 kN-m/m³) (Standard No. ASTM D698-12e2). ASTM International.

ASTM International. (2012), Standard test methods for laboratory compaction characteristics of soil using modified effort (56,000 ft-lbf/ft³; 2,700 kN-m/m³) (Standard No. ASTM D1557-12e1). ASTM International.

ASTM International. (2016), Standard test method for unconfined compressive strength of cohesive soil (Standard No. ASTM D2166/D2166M-16). ASTM International.

ASTM International. (2016), Standard test methods for

measurement of hydraulic conductivity of saturated porous materials using a flexible wall permeameter (Standard No. ASTM D5084-16a). ASTM International.

Ali, M., Aziz, M., Hamza, M. and Madni, M.F. (2020), "Engineering properties of expansive soil treated with polypropylene fibers", *Geomech. Eng.*, **22**(3), 227-236. https://doi.org/10.12989/gae.2020.22.3.227.

Anandha Kumar, S., Sujatha, E.R., Pugazhendi, A. and Jamal, M.T. (2021), "Guar gum-stabilized soil: a clean, sustainable and economic alternative liner material for landfills", *Clean Technol. Environ. Policy*, **25**, 323-341. https://doi.org/10.1007/s10098-021-02032-z.

Andrew, R.M. (2018), Global CO2 emissions from cement production", *Earth System Science Data*, *10*(1), 195–217. https://doi.org/10.5194/essd-10-195-2018

Ayeldeen, M., Negm, A., El-Sawwaf, M. and Kitazume, M. (2017), "Enhancing mechanical behaviors of collapsible soil using two biopolymers", *J. Rock Mech. Geotech. Eng.*, **9**(2), 329-339. https://doi.org/10.1016/J.JRMGE.2016.11.007.

Aziz, M., Sheikh, F.N., Qureshi, M.U., Rasool, A.M. and Irfan, M. (2021), "Experimental study on endurance performance of lime and cement-treated cohesive soil", *KSCE J. Civil Eng.*, **25**(9), 3306-3318. https://doi.org/10.1007/s12205-021-2154-7.

Baghdir, B., Abed, Y., Feia, S., Denine, S., Beyaz, T. and Cherifi, A. (2024), "Effect of Xanthan gum biopolymer combined with fibre as soil-stabilization binder of dune sand in Southern Algeria", *Geomech. Eng.*, **39**(2), 115-127. https://doi.org/10.12989/gae.2024.39.2.115.

Barman, D. and Dash, S.K. (2022), "Stabilization of expansive soils using chemical additives: A review", *J. Rock Mech. Geotech. Eng.* 14(4), 1319-342. https://doi.org/10.1016/J.JRMGE.2022.02.011.

Basma, A., Alhomoud, A. and Altabari, E. (1994), "Effects of methods of drying on the engineering behavior of clays", *Appl. Clay Sci.*, **9**(3), 151-164. https://doi.org/10.1016/0169-1317(94)90017-5.

Biju, M.S. and Arnepalli, D.N. (2020), "Effect of biopolymers on permeability of sand-bentonite mixtures", *J. Rock Mech. Geotech. Eng.*, **12**(5), 1093-1102. https://doi.org/10.1016/j.jrmge.2020.02.004.

Blanck, G., Cuisinier, O. and Masrouri, F. (2014), "Soil treatment with organic non-traditional additives for the improvement of earthworks", *Acta Geotechnica*, **9**(6), 1111-1122. https://doi.org/10.1007/s11440-013-0251-6.

Bouazza, A., Gates, W.P. and Ranjith, P.G. (2009), "Hydraulic conductivity of biopolymer-treated silty sand", *Géotechnique*, **59**(1), 71-72. https://doi.org/10.1680/geot.2007.00137.

Cadmus, M.C., Jackson, L.K., Burton, K.A., Plattner, R.D. and Slodki, M.E. (1982), "Biodegradation of Xanthan gum by Bacillus sp", *Appl. Environ. Microbiol.*, **44**(1), 5-11. https://doi.org/10.1128/aem.44.1.5-11.1982.

Casas, J., Santos, V. and García-Ochoa, F. (2000), "Xanthan gum production under several operational conditions: molecular structure and rheological properties", *Enzyme and Microbial Technol.*, **26**(2-4), 282-291. https://doi.org/10.1016/S0141-0229(99)00160-X.

Chang, I. and Cho, G.C.C. (2014), "Geotechnical behavior of a beta-1,3/1,6-glucan biopolymer-treated residual soil", *Geomech. Eng.*, **7**(6), 633-647. https://doi.org/10.12989/gae.2014.7.6.633.

Chang, I. and Cho, G.C. (2012), "Strengthening of Korean residual soil with β-1,3/1,6-glucan biopolymer", *Constr. Build. Mater.*, **30**, 30-35. https://doi.org/10.1016/j.conbuildmat.2011.11.030.

Chang, I., Im, J. and Cho, G.C. (2016), "Introduction of microbial biopolymers in soil treatment for future environmentally-friendly and sustainable geotechnical engineering", *Sustainability*, **8**(3), 251. https://doi.org/10.3390/su8030251.

Chang, I., Im, J., Prasidhi, A.K. and Cho, G.C. (2015), "Effects of Xanthan gum biopolymer on soil strengthening", *Constr. Build. Mater.*, **74**, 65-72. https://doi.org/10.1016/j.conbuildmat.2014.10.026.

Chang, I., Jeon, M. and Cho, G.C. (2015), "Application of microbial biopolymers as an alternative construction binder for earth buildings in underdeveloped countries", *Int. J. Polymer Sci.*, 1-9. https://doi.org/10.1155/2015/326745.

Chang, I., Prasidhi, A.K., Im, J. and Cho, G.C. (2015), "Soil strengthening using thermo-gelation biopolymers", *Constr. Build. Mater.*, **77**, 430-438. https://doi.org/10.1016/J.CONBUILDMAT.2014.12.116.

Chen, C., Wu, L., Perdjon, M., Huang, X. and Peng, Y. (2019), "The drying effect on xanthan gum biopolymer treated sandy soil shear strength", *Constr. Build. Mater.*, **197**, 271-279. https://doi.org/10.1016/j.conbuildmat.2018.11.120.

Cheng, Z. and Geng, X. (2023), "Investigation of unconfined compressive strength for biopolymer treated clay", *Constr. Build. Mater.*, **385**, 131458. https://doi.org/10.1016/J.CONBUILDMAT.2023.131458.

Chudzikowski, R.J. (1971), "Guar gum and its applications", *J. Soc. Cosmetics Chem.*, **22**(1), 43-60.

Comba, S. and Sethi, R. (2009), "Stabilization of highly concentrated suspensions of iron nanoparticles using shear-thinning gels of xanthan gum", *Water Res.*, **43**(15), 3717-3726. https://doi.org/10.1016/j.watres.2009.05.046.

Das, B.M. and Sobhan, K. (2013), *Principles of Geotechnical Engineering* (8th ed.). Cengage Learning.

Dehghan, H., Tabarsa, A., Latifi, N. and Bagheri, Y. (2019), "Use of xanthan and guar gums in soil strengthening", *Clean Technol. Environ. Policy*, **21**(1), 155-165. https://doi.org/10.1007/s10098-018-1625-0.

Gao, Q.F., Shi, X.K., Zeng, L., Yu, H.C. and Hu, J.X. (2025), "Characterization of the mechanical behavior and stabilization mechanism of soft soil treated with Xanthan gum biopolymer", *Polymers*, **17**(11), 1532. https://doi.org/10.3390/POLYM17111532.

García-Ochoa, F., Santos, V.E., Casas, J.A. and Gómez, E. (2000), "Xanthan gum: production, recovery, and properties", *Biotechnol. Adv.*, **18**(7), 549-579. https://doi.org/10.1016/S0734-9750(00)00050-1.

Ham, S.M., Chang, I., Noh, D.H., Kwon, T.H. and Muhunthan, B. (2018), "Improvement of surface erosion resistance of sand by microbial biopolymer formation", *J. Geotech. Geoenviron. Eng.*, **144**(7), 06018004. https://doi.org/10.1061/(ASCE)GT.1943-5606.0001900.

Hamza, M., Nie, Z., Aziz, M., Ijaz, N., Ameer, M.F. and Ijaz, Z. (2023), "Geotechnical properties of problematic expansive subgrade stabilized with xanthan gum biopolymer", *Road Mater. Pavement Des.*, **24**(7), 1869-1883. https://doi.org/10.1080/14680629.2022.2092027.

Hamza, M., Nie, Z., Aziz, M., Ijaz, N., Ijaz, Z. and Rehman, Z. (2022), "Strengthening potential of xanthan gum biopolymer in stabilizing weak subgrade soil", *Clean Technol. Environ. Policy*, 24(9), 2719-2738. https://doi.org/10.1007/s10098-022-02347-5.

Ivanov, V. and Chu, J. (2008), "Applications of microorganisms to geotechnical engineering for bioclogging and biocementation of soil in situ", *Rev. Environ. Sci. Bio Technol.*, **7**(2), 139-153. https://doi.org/10.1007/s11157-007-9126-3.

Katzbauer, B. (1998), "Properties and applications of xanthan gum", *Polymer Degradation and Stability*, **59**(1-3), 81-84.

Khachatoorian, R., Petrisor, I.G., Kwan, C.C. and Yen, T.F. (2003), "Biopolymer plugging effect: laboratory-pressurized pumping flow studies", *J. Petroleum Sci. Eng.*, **38**(1-2), 13-21.

Khatami, H.R. and O'Kelly, B.C. (2013), "Improving mechanical

properties of sand using biopolymers", *J. Geotech. Geoenviron. Eng.*, **139**(8), 1402-1406.
Knox, A.S., Petrisor, I.G., Turick, C.E., Roberts, J., Paller, M.H., Reible, D.D. and Forrest, C.R. (2010), "Life span of biopolymer sequestering agents for contaminant removal and erosion resistance", (Ed., M.M.M. Elnashar), *Biopolymers*, 1-632. Sciyo. https://doi.org/10.5772/10259.
Kumara, S.A. and Sujatha, E.R. (2020, "Performance evaluation of β-glucan treated lean clay and efficacy of its choice as a sustainable alternative for ground improvement", *Geomech. Eng.*, **21**(5), 413-422. https://doi.org/10.12989/gae.2020.21.5.413.
Lappin-Scott, H.M., Cusack, F. and Costerton, J.W. (1988), "Nutrient resuscitation and growth of starved cells in sandstone cores: a novel approach to enhanced oil recovery", *Appl. Environ. Microbiol.*, **54**(6), 1373-1382.
Latifi, N., Horpibulsuk, S., Meehan, C.L., Abd Majid, M.Z., Tahir, M.M. and Mohamad, E.T. (2017), "Improvement of problematic soils with biopolymer—an environmentally friendly soil stabilizer", *J. Mater. Civil Eng.*, **29**(2), 04016204. https://doi.org/10.1061/(ASCE)MT.1943-5533.0001706.
Latifi, N., Horpibulsuk, S., Meehan, C.L., Majid, M.Z.A. and Rashid, A.S.A. (2016), "Xanthan gum biopolymer: an eco-friendly additive for stabilization of tropical organic peat", *Environ. Earth Sci.*, **75**(9), 825. https://doi.org/10.1007/s12665-016-5643-0.
Lee, S., Chung, M., Park, H.M., Song, K.I. and Chang, I. (2019), "Xanthan gum biopolymer as soil-stabilization binder for road construction using local soil in Sri Lanka", *J. Mater. Civil Eng.*, **31**(11), 06019012. https://doi.org/10.1061/(ASCE)MT.1943-5533.0002909.
MacLeod, F.A., Lappin-Scott, H.M. and. Costerton, J.W. (1988), "Plugging of a model rock system by using starved bacteria", *Appl. Environ. Microbiol*., **54**(6), 1365-1372.
Meo, S.A. (2004), "Health hazards of cement dust", *Saudi Medical J*., **25**(9), 1153-1159.
Moghal, A.A.B. and Vydehi, K.V. (2021), "State-of-the-art review on efficacy of xanthan gum and guar gum inclusion on the engineering behavior of soils", *Innov. Infrastruct. Solu.*, **6**(2), 108. https://doi.org/10.1007/s41062-021-00462-8
Obrzud, R.F. (2010), "On the use of the Hardening Soil Small Strain model in geotechnical practice", *Numer. Geotech. Struct.*, **16**, 1-17.
Onah, H.N., Nwonu, D.C. and Ikeagwuani, C.C. (2022), "Feasibility of lime and biopolymer treatment for soft clay improvement: a comparative and complementary approach", *Arabian J. Geosci.*, **15**(4), 337. https://doi.org/10.1007/s12517-022-09552-y.
Park, J.K. and Yen, T.F. (1994), "Subsurface application of slime-forming bacteria in soil matrices", *Appl. Biotechnol. Site Remediation*, **2**, 268.
Peethamparan, S. and Olek, J. (2008), "Study of the effectiveness of cement Kiln dusts in stabilizing Na-montmorillonite clay", *J. Mater. Civil Eng.*, **20**(2), 137-146. https://doi.org/10.1061/(ASCE)0899-1561(2008)20:2(137).
Perkins, S.W., Gyr, P. and James, G. (2000), "The influence of biofilm on the mechanical behavior of sand", *Geotech. Test. J.*, **23**(3), 300-312.
Petri, D.F.S. (2015), "Xanthan gum: A versatile biopolymer for biomedical and technological applications", *J. Appl. Polymer Sci.*, **132**(23), 1-13. https://doi.org/10.1002/app.42035.
Qureshi, M.U., Alsaidi, M., Aziz, M., Chang, I., Rasool, A.M. and Kazmi, Z.A. (2021), "Use of reservoir sediments to improve engineering properties of dune sand in Oman", *Appl. Sci.*, **11**(4), 1620. https://doi.org/10.3390/app11041620.
Ramachandran, S.K., Ramakrishnan, V. and Bang, S.S. (2001),. Remediation of concrete using micro-organisms", *ACI Mater. J*., **98**(1), 3-9.
Rasool, A.M., Hameed, A., Qureshi, M.U., Ibrahim, Y.E., Qazi, A.U. and Sumair, A. (2023), "Experimental study on strength and endurance performance of burnt clay bricks incorporating marble waste", *J. Asian Architect. Build. Eng.*, **22**(1), 240-255. https://doi.org/10.1080/13467581.2021.2024203.
Rosalam, S. and England, R. (2006), "Review of xanthan gum production from unmodified starches by Xanthomonas comprestris sp", *Enzyme Microbial Technol.*, **39**(2), 197-207. https://doi.org/10.1016/j.enzmictec.2005.10.019.
Sujatha, E.R., Sudha, B., Aswiin Kumar, M. and Kannan, G. (2025), "Comparative study on the effect of high and low viscous biopolymers for dust suppression – an experimental investigation", *Geomech. Eng.*, **40**(1), 23-32. https://doi.org/10.12989/gae.2025.40.1.023.
Zhang, X., Cao, W. and Zhang, X. (2024), "Experimental study on mechanical and hydraulic properties of xanthan gum improved low liquid limit silty soil", *Scientific Reports*, **14**(1), 11072. https://doi.org/10.1038/s41598-024-61875-w.
Zohuriaan, M.J. and Shokrolahi, F. (2004). "Thermal studies on natural and modified gums", *Polymer Test.*, **23**(5), 575-579. https://doi.org/10.1016/j.polymertesting.2003.11.001.

JS